On optimization of interference fit assembly

Pedersen, Niels Leergaard

Published in:
Structural and Multidisciplinary Optimization

Link to article, DOI:
10.1007/s00158-016-1419-0

Publication date:
2016

Document Version
Peer reviewed version

Noname manuscript No.
(will be inserted by the editor)

On Optimization of Interference Fit Assembly

Niels L. Pedersen

Received: date / Accepted: date

Abstract Assembly of shaft and hub by an interference fit is a classical connection with known advantages and disadvantages. The advantage being the level of possible torque transfer while the disadvantage is a possible fretting fatigue failure at the points of stress concentration. To improve the assembly the present paper discusses different optimized designs that improve the contact pressure distribution. The pressure distribution in the contact is the source responsible for the fatigue failure. The distribution can be improved by design modification done directly on the contacting surfaces which however requires a very high production precision. Alternatively it is shown, how hub side shape optimization can improve the pressure distribution significantly. The latter design change has no influence on the remaining shaft-hub design i.e. the attachment of other parts. The analysis is performed either by a traditional contact analysis, or by a super element contact analysis where no iterations are needed for the contact evaluation.[1]

Keywords Interference fit · Contact · Shape optimization · Stress concentration · FE

1 Introduction

Interference fit or press fit is one of the most used assembly methods for shaft-hub connection. This type of assembly is superior with respect to possible torque transmission between two assembled parts. The disadvantage is that in a typical configuration disassembly is not possible. The limit that dictates if an interference fit is possible is typically either the maximum possible heating or cooling of the parts during the assembly process or the stress in the connection in operation. Once assembled the interference fit may fail due to fretting fatigue. Fretting fatigue is a type of fatigue where the parts fail due to relative movement/sliding between compressed parts. The failure is a gradual surface deterioration resulting in loss of contact pressure. Experimental verification of fretting fatigue can be found in Alfredsson (2009) and the residual stress in an interference fit is discussed in Gamer and Lance (1983)

In a traditional design with cylindrical assembly surfaces for shaft and hub, the result is a large stress concentration at the axial ends of contact. The shaft is in the working condition typically loaded in both bending and torsion. The combination of the high stress and the relative motion result in the fretting fatigue. Results found in Reusner (1987) and Fujiwara and Kawase (2007) indicate that for roller bearings, although not directly comparable, it is possible to achieve a constant contact pressure by special roller design. Design changes to the interference fit contact surfaces should therefore also be possible. In the literature many different design changes have been proposed for improving the interference fit strength, different ways of changing the contact can be found in e.g. Nishioka and Komatsu (1967), White and Humpherson (1969), Hattori et al (1981), Lee et al (2010), Kataoka et al (2007) and Biron et al (2013). Improving the interference design by shape changes made to the hub can be found in Nishioka and Komatsu (1967) and Juuma (2000). The effect of a stress relief groove on fretting fatigue strength is stud-

Niels L. Pedersen
Dept. of Mechanical Engineering, Solid Mechanics
Technical University of Denmark
Nils Koppels Allé, Building 404, DK-2800 Kgs. Lyngby, Denmark
E-mail: nlp@mek.dtu.dk

[1] Part of the work was presented at the WCSMO-11 conference in Sydney, Australia, 2015.

ied extensively in the paper by Kubota et al (2009), the results show that due to the high stresses at the groove edge, the groove edge and the counter part in the hub is progressively removed due to fretting fatigue resulting in an opening between the two parts.

How the shape of an optimal contact pressure should be might not have a straight forward answer. If fretting fatigue is to be avoided then there should be no relative motion between the two parts in contact, the possibility for relative motion is controlled by the friction coefficient and the normal pressure, therefore one could argue that the contact pressure at the contact end should be high. This reasoning have lead to the suggested design improvement where, e.g., there is a groove in the shaft and simultaneously the hub has an overhang over part of this groove leading to an even higher stress concentration at the end of contact. On the other hand if there is relative motion between two parts in contact then the contact pressure should be low in order to avoid fretting fatigue. As seen in the paper by Kubota et al (2009) the high stress values can result in deterioration of either the hub or the shaft or both due to the high stress. The interference fit should function when the connection is loaded; typically both in bending and torsion. The torsion only creates shear stress and the contact pressure in the connection is not affected by the torsion, therefore for a pure torsional load the design criteria is that the contact pressure is so high that relative motion is avoided and at the same time so that the von Mises stress is lower than the yield stress. For the interference fit in bending the contact pressure is increased and reduced during the rotation. The traditional design has a stress concentration and it seems that even though the stress is high at the end of contact, the contact pressure will either be increased to a too high level due to the bending or reduced to a too low level that allow for relative motion between the parts. The specific choice made in the present paper is; that the design objective is to have a constant contact pressure between the parts. The objective is therefore not to reduce the overall interference but to improve the condition for increasing the average interference in the connection and thereby increase the limit for external load on the connection. The contact pressure size should be selected such that the fretting fatigue is avoided and on the other hand as high as possible to fully take advantage of the interference fit.

A constant contact pressure between the parts can be achieved in different ways; one possibility is to make changes to the contacting surfaces, however as it will be demonstrated the variation in the diameters are in the order of μm, resulting in a very high production price relative to the normal production methods. Alternatively the design optimization/modification can be made to the hub side. By making the design modification here we can achieve significant improvements and simultaneously the shaft-hub connection can be manufactured in the traditional way. The analysis of contact pressure is performed using the finite element method and includes contact analysis. The number of design variables is limited facilitating that the optimization can be performed using a parameter study. The limited number of design variables is argued from a machine elements point-of-view, i.e. the results must be practical attainable and easily communicated to the designer.

The paper is organized as follows. Section 2 discuss the stress singularity of the traditional design and compares this to the traditional 2D analytical result. In Section 3 a super element technique for determining the interference for given pressure or pressure for given interference is presented. Applying the simple formulation two hub design modifications are presented. A full contact analysis is performed in Section 4 the starting point is the optimized design found in Section 3. The overall result is that a constant or near constant contact pressure can be obtain in an interference fit by modification made to the hub side.

2 Stress singularity of standard design

For a standard interference fit the contacting surface design is specified by the diameter and tolerance on the shaft and hub, i.e. a typical design could have a tolerance `H7/u6` indicating that the hole tolerance is `H7` and the shaft tolerance is `u6`. Depending on the fit diameter these types of specification result in a constant interference along the contact line of a given size. This type of design is known to give a stress concentration at the connection ends, see e.g. Nishioka and Komatsu (1967), Kataoka et al (2007), Truman and Booker (2007), Gutkin and Alfredsson (2008) and Lee et al (2013).

The stress at singularities can be estimated in different ways analytically or numerically depending on the specific discipline, e.g. in fracture mechanics or within plasticity modeling. For welded structures a known method is the hot spot method, see e.g. Poutiainen et al (2004) and references therein. To evaluate the stress singularity size in the present paper a FE model with a mesh refinement at the point of stress concentration is used. Reducing the element size at the singularity will increase the maximum stress and the stress size will approach infinity as the element size goes to zero.

The data for the shaft and hub connection used in the present paper is

– Shaft: length $L_s = 0.6$m, diameter $D_f = 0.2$m
– Hub: length $L_h = 0.3$m, inner diameter $D_i = 0.2$m and outer diameter of hub $D_h = 0.4$m

The interference is introduced in the finite element model by modeling a hub cooling of 100°C. The hub and shaft elastic properties are assumed identical and given by

$$E = 2.1 \cdot 10^5 \text{MPa}, \qquad \nu = 0.3, \qquad \alpha = 1.1 \cdot 10^{-5}/^\circ\text{C}$$

where E is modulus of elasticity, ν is Poisson's ratio and α is the thermal expansion coefficient. With a tolerance `H7/u6` and the given data this fit corresponds to an interference fit between $\delta_d = 190\mu$m and $\delta_d = 265\mu$m. A cooling or heating of one component by 100°C results in a fit of $\delta_d = 220\mu$m. The classical analytical pressure in the connection, under the assumption of axis symmetry and plane stress, is given by

$$p_f = \frac{E\delta_d}{2D_f}\left(1 - \left(\frac{D_f}{D_h}\right)^2\right) \tag{1}$$

With the given data the pressure is $p_f = 86.6$MPa. This pressure corresponds to a maximum von Mises stress in the hub of $7/3 \cdot p_f$.

The singularity size for the present design is estimated using the COMSOL program (COMSOL AB (1998-2009)). The connection is modeled assuming axis symmetry as seen in Figure 1. In the contact modeling it is first examined if the inclusion of friction is important for the pressure evaluation, from the computation it is found that the friction does have an influence but that it has a negligible influence on the contact pressure, therefore the remaining computations are performed without friction.

Using the finite element method to evaluate the stress at the sharpe corner in an interference fit will as indicated result in the traditional problem; the stress in the corner will not converge by refining the mesh, the stress will in the limit be infinite. In order to evaluate the stress concentration factor it is therefore here selected to identify the stress 10μm from the hub edge.This size is of cause a compromise but selecting a smaller number will increase the finite element model and the size is comparable to surface roughness. The specific size of the stress concentration is not the focus of the present paper, the primary use is to see the relative reduction/change in the maximum stress for design revisions. The overall stress distribution is shown in Figure 2a and in Figure 2b a zoom of the last 1mm of the contact is shown. The finite element model is highly refined with 30 FE nodes along the last 10μm of the contact

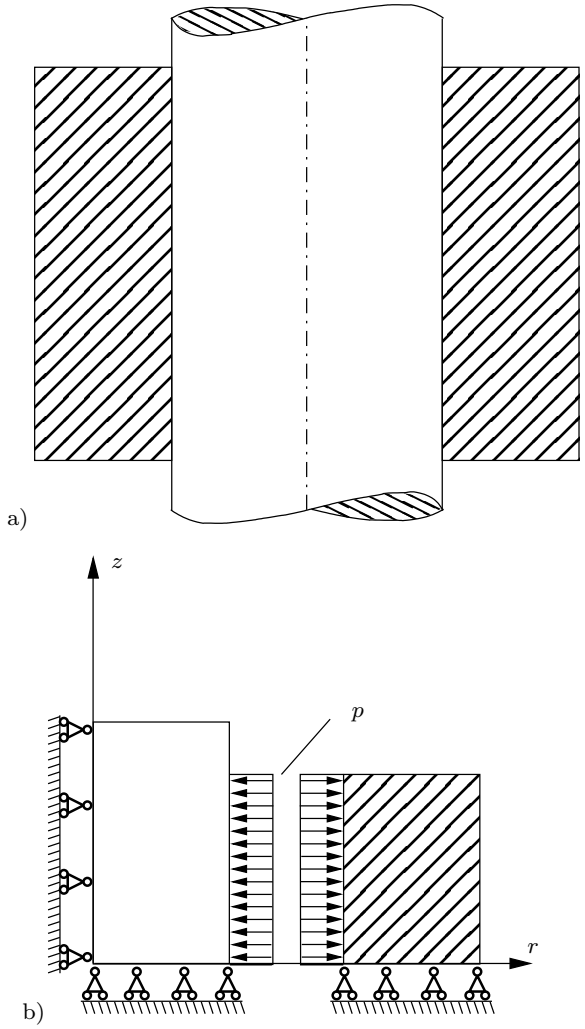

Fig. 1 a) The interference fit. b) Illustration of the axis symmetric model of half the shaft and hub used in the analysis. The contact pressure p is to be determined from the analysis, the shown constant distribution is used here only for illustration purposes.

in Figure 2a and in the shown zoom with 60 FE nodes along the last 10μm. The contact stress (10μm from the hub edge) is by finite element mesh refinement found to converge to a level of 415MPa. From the computation we conclude that the theoretical contact stress concentration factor K_{tc} for this case is

$$K_{tc} \approx \frac{415}{86.6} = 4.8 \tag{2}$$

The exact value of the theoretical stress concentration factor can always be discussed, but it is clear that the stress concentration has a significant size. The maximum von Mises stress 10μm from the hub edge is 516MPa. If we therefore instead express the stress

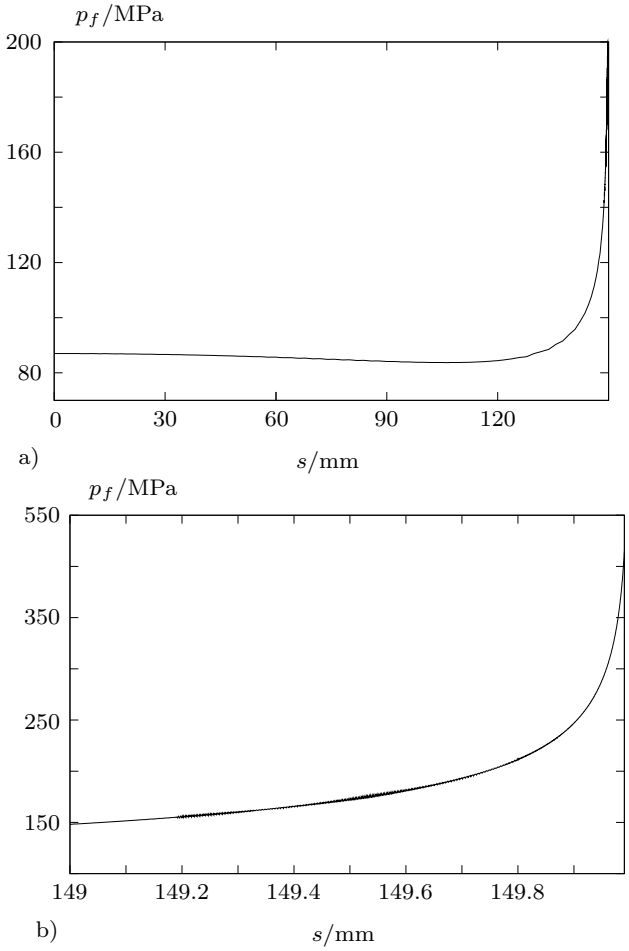

Fig. 2 Contact pressure along interference fit. a) Full length of contact. b) Zoom of last 1mm of contact, the stress is not plotted for the last 10μm due to the singularity, the maximum stress 10μm from the edge is 415MPa.

concentration in the von Mises stress we find a smaller value.

$$K_t \approx \frac{516}{7/3 \cdot 86.6} = 2.55 \tag{3}$$

In relation to fretting fatigue it is however the contact stress that is of primary interest.

3 Super element technique for contact analysis

An alternative to performing contact analysis by a traditional iterative finite element analysis (FEA) is to use the super element technique. The procedure involves no iterations see Pedersen (2006a). Application of the method for shrink fit analysis can be found in Pedersen (2006b) and in relation to bolted connection see Pedersen and Pedersen (2009). The primary advantage of the method is that no iterations are needed in the FE calculation, for an easy reference the procedure is shortly presented here. In Figure 1a an interference fit is shown. The axis symmetric model of half the connection is also shown in Figure 1b together with a contact pressure distribution.

In the analysis the shaft and hub are separated. The super element FE hub model is given as

$$[S_{hp}]\{D_{hp}\} = \{F_{cp}\} \tag{4}$$

where $[S_{hp}]$ is the hub super element stiffness matrix. The order of this matrix equals the number of FE mesh nodes on the contact line. The resulting contact node displacements in the radial direction are given by $\{D_{hp}\}$ and the corresponding nodal contact pressure forces are given in $\{F_{cp}\}$. The total contacting force is given as the nodal force sum, $F_p = ||\{F_{cp}\}||_1$, with respect to practical issues related to super element matrix determination see Pedersen (2006a).

It is assumed that the contact line on the shaft has the same number of nodes (mutual corresponding) as the hub contact line. The analysis for the shaft can under this assumption be performed in a similar manner using the super finite element matrices for this part.

$$[S_{sp}]\{D_{sp}\} = -\{F_{cp}\} \tag{5}$$

where $[S_{sp}]$ is the shaft super element stiffness matrix. The order of this matrix also equals the number of FE mesh nodes on the contact line. The resulting contact node displacements are given by $\{D_{sp}\}$ and the corresponding nodal contact pressure forces are given by $-\{F_{cp}\}$, i.e., a negative sign relative to the hub analysis to express equilibrium with (4).

Before assembly the radial interference (negative gap) between the shaft and hub for the nodes on the line of contacts can be given as

$$\{\delta\} = \{r_s\} - \{r_h\} \tag{6}$$

where $\{r_s\}$ and $\{r_h\}$ are the radial node positions on the contact line for the shaft and hub respectively. After the two components are fitted together the nodes will be at the same point, i.e. we have that

$$\{r_s\} + \{D_{sp}\} = \{r_h\} + \{D_{sh}\} \Rightarrow \{\delta\} = \{D_{sh}\} - \{D_{sp}\} \tag{7}$$

The super element technique can be used in two different ways; either the contact force distribution, $\{F_{cp}\}$,

is assumed know and from this the interference, $\{\delta\}$, can be found directly by

$$\{\delta\} = ([S_{hp}]^{-1} + [S_{sp}]^{-1})\{F_{cp}\} \tag{8}$$

alternatively the interference is assumed known and the contact force can be found from

$$\{F_{cp}\} = ([S_{hp}]^{-1} + [S_{sp}]^{-1})^{-1}\{\delta\} \tag{9}$$

The result we achieve is that under the given assumptions the contact force can be found directly without iterations from a given interference distribution. The analysis involved the inverse matrix determination for the two super finite element stiffness matrices, but the size of these is limited to the number of nodes on the contact line.

3.1 Design modification of contact zone

Under the assumption used in (8) we may find the interference $\delta(z)$, as a function of the position z, that will result in a constant stress. In Figure 3 the resulting interference for the shaft hub design used in the present paper with a constant pressure of 86.6MPa is shown.

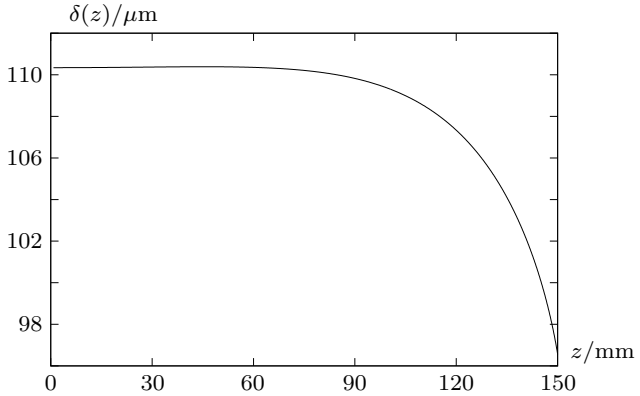

Fig. 3 Interference as a function of axial position (see Figure 1) that result from a constant (uniform) pressure, 86.6MPa, in the interference fit.

There is no limit to the pressure complexity for this procedure, any given variation can be analyzed and the resulting interference can be found in a rather simple manner.

As can be seen in Figure 3 the variation in the interference is not very high as compared to the normal production methods where the interference is specified by tolerances, the variation lies in this case within 14μm. Creating a shaft and hub with exactly the shown interference is therefore not feasible.

The results indicate that the connection for a constant interference, $\delta(z) = \delta_{\text{const.}}$, is too stiff at the hub side. One way of changing this assuming that a constant interference is used is to make design changes to the hub side.

3.1.1 Chamfered design

A simple design change is to make a hub chamfer as seen in Figure 4a. The optimization problem can be stated as minimize the variation in the interference for a given constant pressure. The optimized interference for this design change is shown in Figure 4b. The given simple design parameterization does not allow for a completely constant interference.

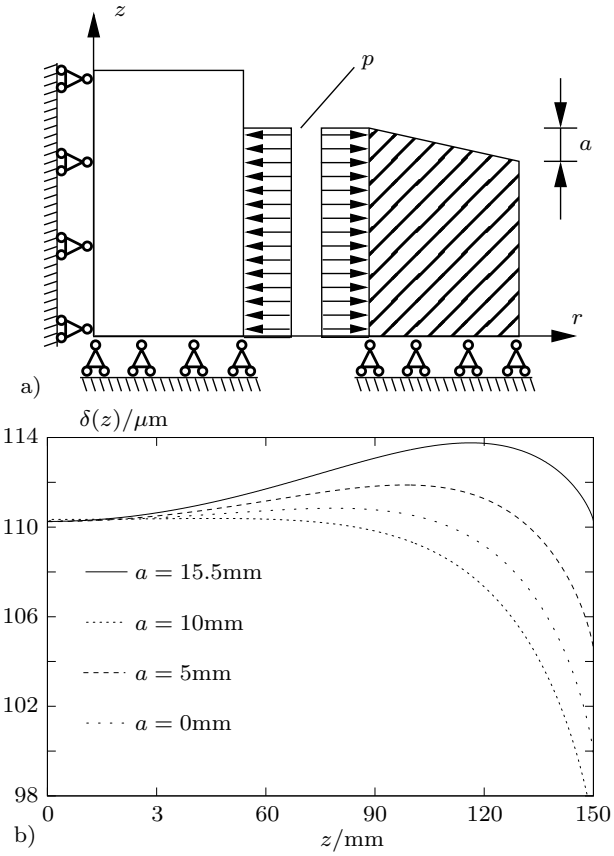

Fig. 4 a) Simple chamfer design of hub. b) Interference as a function of axial position for different chamfer size that result from a constant (uniform) pressure, 86.6MPa, in the interference fit.

In Figure 4b the best chamfer value is seen to be $a =$ 15.5mm which gives a total variation in the interference of 3.5μm to be compared to the original 14μm for no

chamfer $a = 0$mm. The optimized value of a is found by a parameter study.

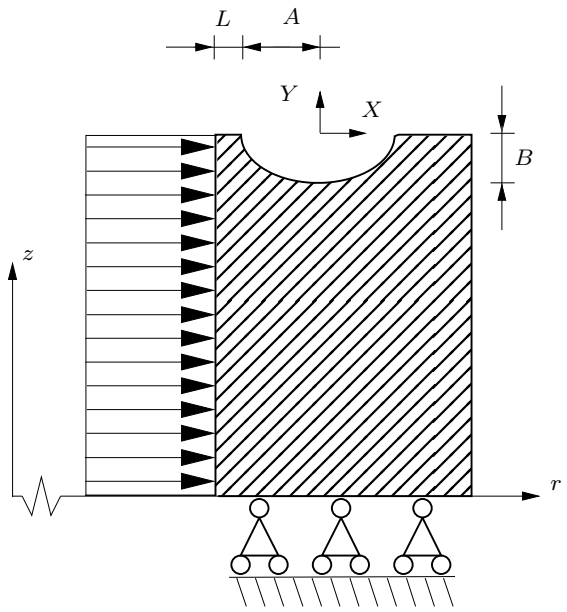

Fig. 5 Parameterization of super elliptical cut in hub side.

One disadvantage, the presented chamfer design has, is the reduction in the possible use of the hub, e.g., we can not use the whole length for a gear.

3.1.2 Super elliptic design

An alternative design change is to use a super elliptical cut in the hub side. In Figure 5 the design parameterization for the elliptical cut is shown.

The super ellipse (with principle axes A and B and super elliptical power η) is in parametric form (for half the shape) given by

$$X = A\cos(t)^{(2/\eta)}, \qquad t \in [0 : \frac{\pi}{2}] \tag{10}$$

$$Y = -B\sin(t)^{(2/\eta)}, \qquad t \in [0 : \frac{\pi}{2}] \tag{11}$$

where the shape is assumed symmetric relative to the Y-axis in Figure 5.

The optimization is performed as a parameter study with the design parameters A, B, L and η, and the objective is again to achieve an interference/gap that is constant. An optimized design is found for $A = 30$mm, $B = 6$mm, $L = 6.1$mm and $\eta = 2.51$. The interference variation is shown in Figure 6, and the optimized interference variation is found to be within 1.07μm as compared to the original with a 14μm variation.

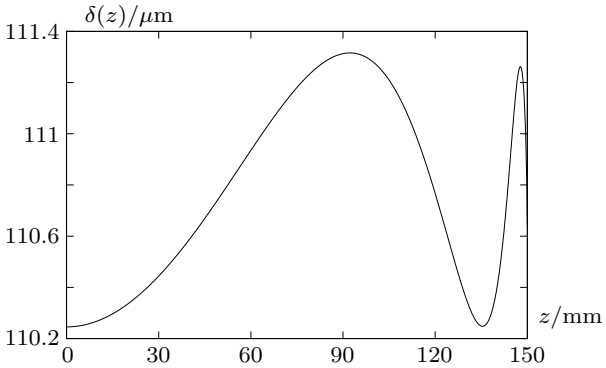

Fig. 6 Interference as a function of axial position for the optimized elliptical cut in the hub side, that result in a constant pressure, 86.6MPa, in the interference fit.

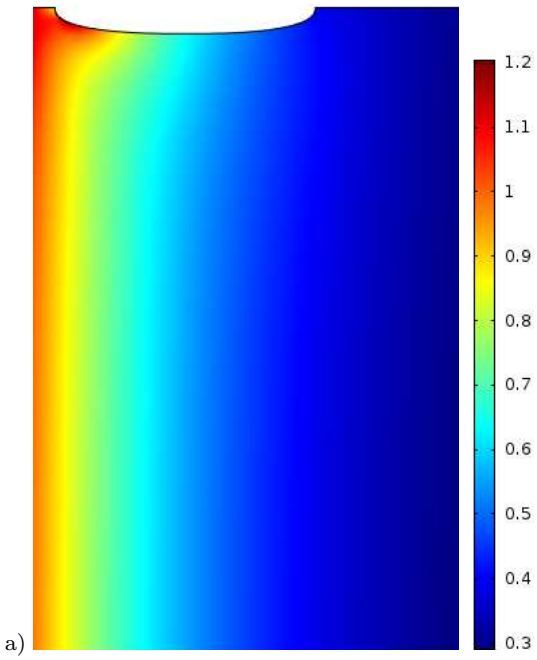

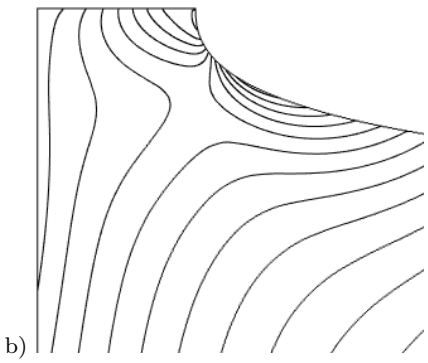

Fig. 7 Von Mises stress in hub from constant internal pressure, the stress have been normalized by $(7/3) \cdot 86.6$MPa $=$ 202MPa. a) Color plot b) Zoom of stress concentration (contour plot).

The von Mises stress of the design is given in Figure 7. Relative to the original design and the design with a chamfer this design change gives rise to a stress concentration at the hub side. The theoretical stress concentration factor (von Mises stress) is $K_t = 1.2$, i.e., much smaller than the stress concentration of $K_t = 2.55$ of the original design.

4 Optimization using contact modeling

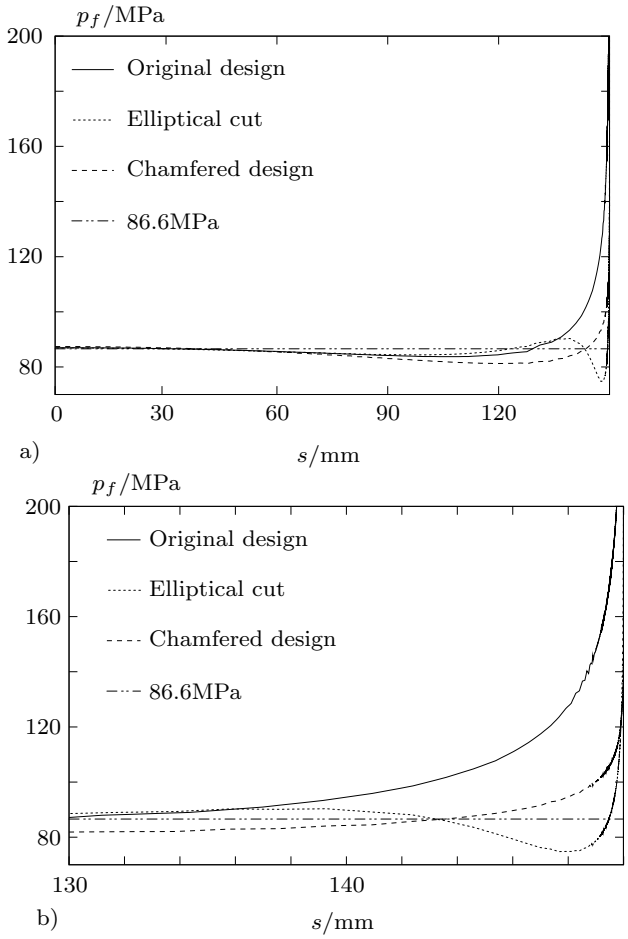

Fig. 8 Contact pressure along interference fit for three different hub designs. a) Full length of contact. b) Zoom of last 20mm of contact, the stress is not plotted for the last 10μm due to the singularity.

The optimized results presented in Section 3 were based on some assumed simplification. First of all the influence of relative sliding between the two surfaces in contact was neglected and the involved friction was also neglected. The results show that the variation of the interference has a size order that do not facilitate practical production, when the goal of the parameter studies was to achieve a constant pressure. To examine the designs we now assume that the interference is constant and do a full contact analysis, i.e. the design changes are limited to the hub side.

In Figure 8 the contact pressure for the original design, the chamfered design and the design with a super elliptical cut is shown, assuming a constant interference. In the figure we also show the analytical constant stress of 86.6MPa for comparison. A hub cooling by 100°C is used to model the interference. It is clearly seen that for both modified designs the pressure distribution is closer to being constant than for the original design. There is however still a rather large variation in the pressure. This is to be expected since the achieved designs did not result in a constant interference. For all the cases the contact analysis have been done with a friction coefficient of $\mu = 0.1$ or without friction, overall the resulting contact pressure is the same and therefore friction is neglected in the remaining part

A closer contact pressure inspection in Figure 8 corresponds very well with the interference variations found previously; the chamfered design results in a smaller contact pressure as compared to the original design over approximately the last 10mm of contact, while the contact pressure for the elliptical cut design has a closer to constant pressure. For all three cases shown in Figure 8 there is a stress singularity at the end.

The hub side shape optimization result depends on the physical nature of the problem, but of cause also on the selected shape parameterization complexity. Here a rather simple parameterization approach is used. This has two benefits; it is easy to communicate the design and this also gives the results a more practical nature which is important from a machine elements point-of-view.

4.1 Shape optimization of hub side

To improve the design further the optimization is also performed using the full contact modeling, we here assume the interference to be constant. Due to the longer computational time a simple design is first considered, the design is shown in Figure 9. The parameterization consists of only two parameters L and B. This design is chosen due to the chamfered designs benefit, i.e., the possibility of removing the stress concentration at the contact end while the cut of at the distance L facilitates that the hub outer part can remain unchanged.

From a strength point-of-view the design in Figure 9 is infeasible, since the sharp corner will cause infinite stress. The design optimization therefore for this case only focuses on the contact stress, the optimized

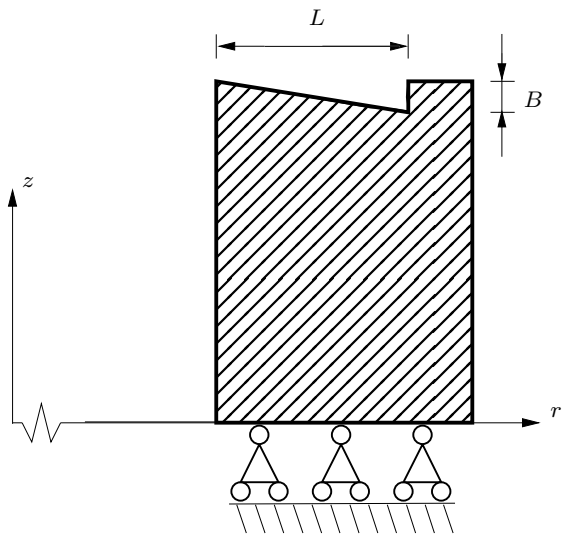

Fig. 9 Illustration of simple parameterization used for analysis with full contact analysis.

simple design will later be changed and primarily serve as an important initial guess. The design is evaluated and optimized in the following relative to the minimum variation in the contact pressure Δp_f defined as

$$\Delta p_f = \max(p_f) - \min(p_f) \tag{12}$$

By varying the parameter L and finding the optimal value of B the relationship in Figure 10 is found.

From Figure 10 some general conclusions can be made. The optimal design parameter values are $L =$ 56mm and $B = 12.8$mm. From Figure 10b we see a linear relation between B and L indicating that the optimal design has a constant chamfer angle. So if there are specific requirements on the maximum value of L the corresponding optimal value of B can be easily found.

The important result here is that the variation in the contact pressure, Δp_f, is seen to be relatively small as compared to the nominal contact pressure of 86.6MPa.

To identify if the optimum values are specific for the given dimensions the hub dimensions have been changed to see if this has an influence on the optimal design parameter values. Increasing either the outer diameter to $D_h = 0.6$m, or alternative increasing the length to $L_h = 0.4$m had no influence on the optimal value of B and L, i.e., the contact pressure variation minimization is primarily related to the local phenomena of removing the stress concentration.

To improve the design further, i.e. by removing the stress concentration at the sharp corner, it is chosen to combine the chamfered design with the elliptical design. The parameterization is shown in Figure 11. The design parameters for the design are A, B, L and η.

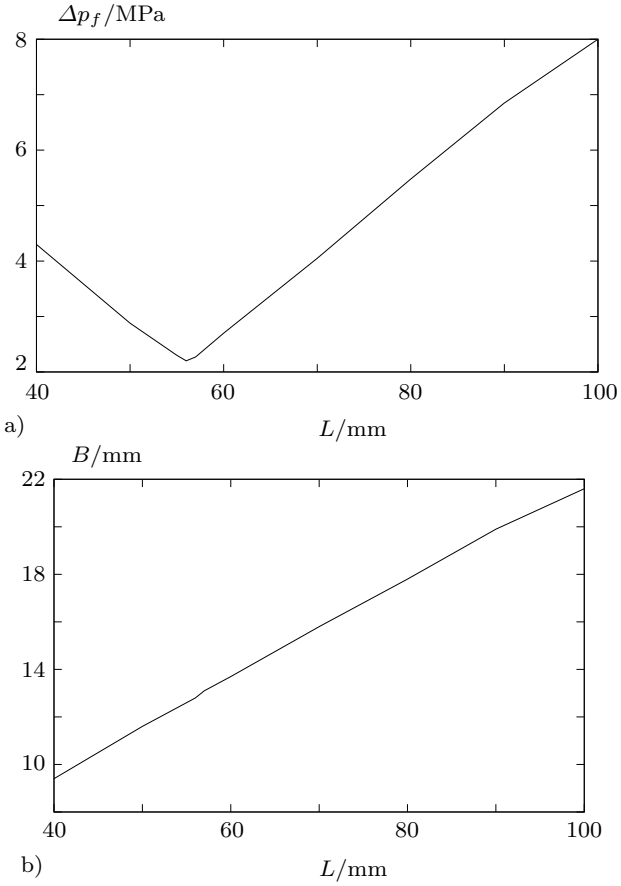

Fig. 10 a) Optimal value of variation in the contact pressure for the optimal design as a function of the design parameter L. b) Optimal value of design parameter B as a function of the design parameter L.

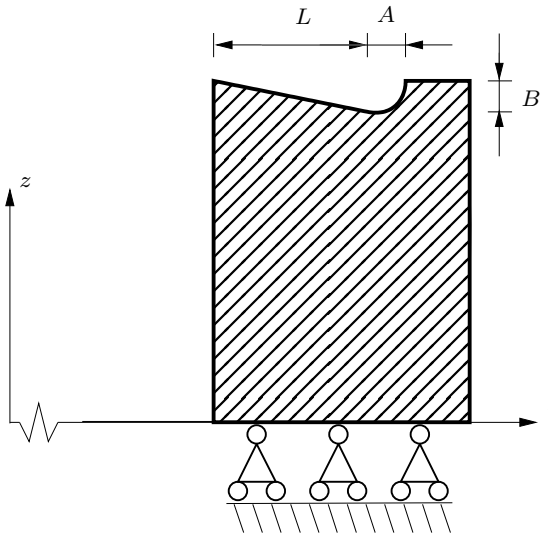

Fig. 11 Illustration of parameterization of combined chamfer and distorted super elliptical cut in hub side.

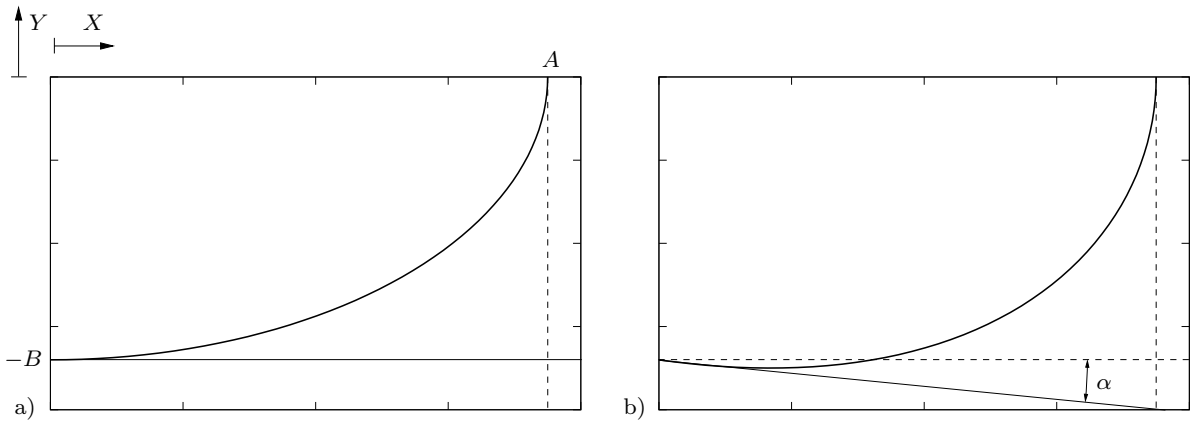

Fig. 12 a) Super ellipse. b) Double distorted super ellipse.

In order to achieve a continuation in the first derivative of the shape the super ellipse is distorted, as it may also be found in Pedersen (2010). The principle behind the distorted super ellipse is shown in Figure 12. The design can be visualized as a rotation of the tangent to the super ellipse by an angle α. The angle α is given by

$$\tan(\alpha) = \frac{B}{L} \tag{13}$$

The distorted super ellipse (with principle axes A and B and super elliptical power η) is in parametric form given by

$$X = A\cos(t)^{(2/\eta)}, \qquad t \in [0 : \frac{\pi}{2}] \tag{14}$$

$$Y = -B(1 + \frac{A}{L}\cos(t)^{(2/\eta)})\sin(t)^{(2/\eta)}, \qquad t \in [0 : \frac{\pi}{2}] \tag{15}$$

The simple parameterization facilities also in this case a rather simple parameter optimization. The influence from variation in the super elliptical power η on the pressure variation is rather limited and it is therefore selected here to use a value of $\eta = 2$. The reason for including the ellipse in the design is to remove the stress concentration at the sharp corner on the hub side. The influence from the design that includes the distorted ellipse as compared to the simple design on the optimal pressure distribution is relatively small, so the contribution of including the distorted ellipse is only related to the stress concentration at the sharp corner. If other values of B and L is selected due to requirements on the design the elliptical design can also in these cases be added to the chamfer to remove the problem with the stress concentration at the corner.

The optimal design is shown in Figure 13, the optimal design is found for the specific values; $L = 53$mm, $B = 12.2$mm, $A = 4$mm and $\eta = 2$. The von Mises stress is shown in Figure 13a where the stress have been normalized by 202MPa. In Figure 13b a normalized von Mises stress contour plot is shown.

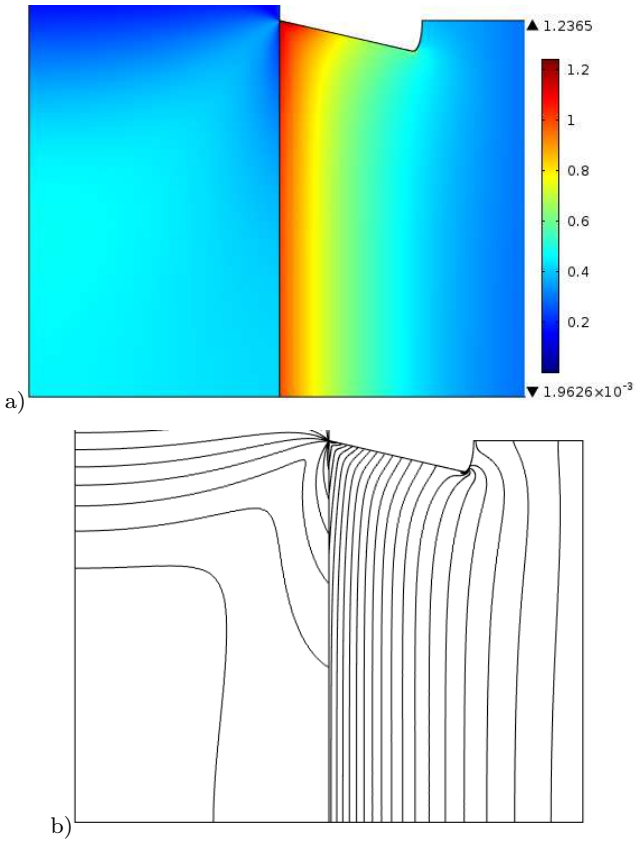

Fig. 13 Optimized design of hub side and the Von Mises stress in hub and shaft from contact modeling, the stress have been normalized by $(7/3)\cdot 86.6$MPa $= 202$MPa. a) Color plot. b) Contour plot.

The related pressure distribution is given in Figure 14. The variation in the pressures is $\Delta p_f = 2.3$MPa and the stress concentration factors are negligible; for the contact pressure it is $K_{tc} = 1.003$ and for the von Mises stress it is $K_t = 1.24$.

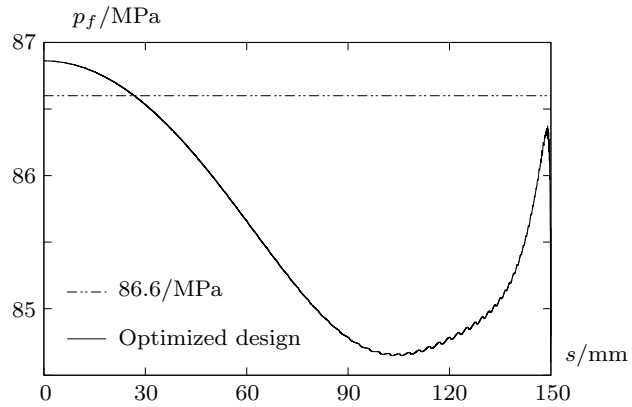

Fig. 14 Contact pressure along interference fit for optimized hub design (please note that the 86.6MPa is the analytical found constant pressure when there is no design changes).

A zoom of the optimized ellipse design is shown in Figure 15. Comparing Figure 15 with Figure 13a it is seen that the stress concentration at the hub side is smaller that that found in the contact.

5 Conclusion

The optimal contact pressure distribution in an interference fit is the objective of optimization. Using a simple super element technique it is found that in order to achieve a constant contact pressure between shaft and hub it is necessary to make variation in the fit diameters in the order of μm which is smaller that the usual tolerance gap specified for the production of interference fits. It is therefore concluded that design changes to the contacting surfaces, i.e. the interference shape variation, are not feasible.

Instead it is shown that the stress concentration present at the end of contact can be reduced or removed by specific design (shape) changes to the hub side. In the example a variation in the contact pressure on the order of 2MPa relative to a nominal pressure of 86MPa is found using a simple hub side shape parameterization with only three active design parameters.

In the present paper the objective is to have a constant stress distribution, but the methods applied can be used for any desired distribution, limited to what is physical obtainable and the shape variation enabled by the selected shape parameterization.

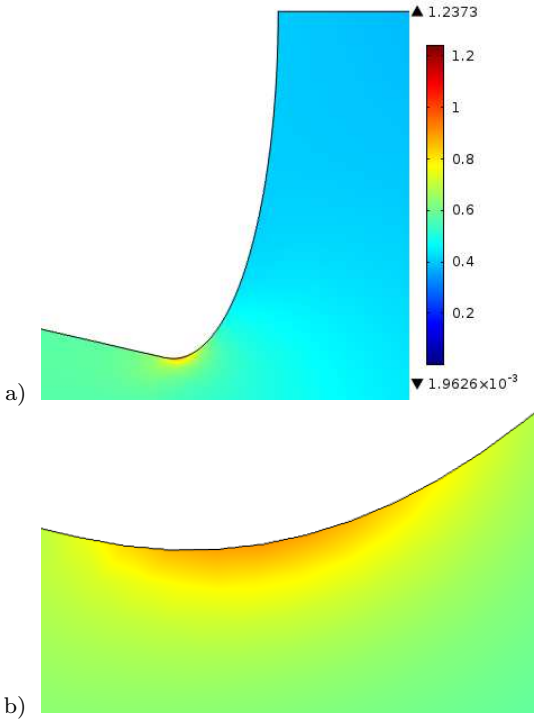

Fig. 15 Normalized von Mises stress. a) elliptical design. b) Zoom of stress concentration in elliptical design part.

Acknowledgements For discussions and suggestions I wish to thank Prof. Peder Klit and Prof. Pauli Pedersen.

References

Alfredsson B (2009) Fretting fatigue of a shrink-fit pin subjected to rotating bending: Experiments and simulations. International journal of fatigue 31(10):1559–1570, DOI 10.1016/j.ijfatigue.2009.04.019

Biron G, Vadean A, Tudose L (2013) Optimal design of interference fit assemblies subjected to fatigue loads. Structural and multidisciplinary optimization 47(3):441–451, DOI 10.1007/s00158-012-0836-y

COMSOL AB (1998-2009) Stockholm, www.comsol.se

Fujiwara H, Kawase T (2007) Logarithmic profiles of rollers in roller bearings and optimization of the profiles (reprint from the original paper (in japanese) carried in the proceedings of the japan society of mechanical engineers part c, vol 72 (2006),3022-2029). NTN Technical review 70:140–148

Gamer U, Lance RH (1983) Residual stress in shrink fits. International Journal of Mechanical Sciences 25(7):465–470

Gutkin R, Alfredsson B (2008) Growth of fretting fatigue cracks in a shrink-fitted joint subjected to rotat-

ing bending. Engineering failure analysis 15(5):582–596, DOI 10.1016/j.engfailanal.2007.04.003

Hattori T, Kawai S, Okamoto N, Sonobe T (1981) Torsional fatigue strength of a shrink fitted shaft. Bulletin of the JSME 24(197):1893–1900

Juuma T (2000) Torsional fretting fatigue strength of a shrink-fitted shaft with a grooved hub. Tribology international 33(8):537–543, DOI 10.1016/s0301-679x(00)00102-x

Kataoka S, Sakae C, Kubota M, Kondo Y (2007) Effect of stress relief groove shape on fretting fatigue strength. Key Engineering Materials 353-358(PART 2):856–859

Kubota M, Kataoka S, Kondo Y (2009) Effect of stress relief groove on fretting fatigue strength and index for the selection of optimal groove shape. International journal of fatigue 31(3):439–446, DOI 10.1016/j.ijfatigue.2008.07.007

Lee DH, Kwon SJ, Seo JW, You WH (2010) Effects of hub contact shape on contact pressure and fatigue life in a press-fitted shaft. Materials Science Forum, Mater Sci Forum 654-656:1638–1641, DOI 10.4028/www.scientific.net/msf.654-656.1638

Lee DH, Choi HY, Song CY, Lee BG (2013) Design of stress relief groove on a press-fitted assembly. Materials processing and manufacturing iii, pts 1-4 753-755(753-755):1339–1342, DOI 10.4028/www.scientific.net/AMR.753-755.1339

Nishioka K, Komatsu H (1967) Researches on increasing the fatigue strength of press-fitted shaft assembly. Bulletin of the Japan Society of Mechanical Engineers 10(42):880–889

Pedersen NL (2010) Improving bending stress in spur gears using asymmetric gears and shape optimization. Mechanism and Machine Theory 45(11):1707–1720

Pedersen NL, Pedersen P (2009) Bolt-plate contact assemblies with prestress and external loads: Solved with super element technique. Computers and Structures 87(21-22):1374–1383, DOI 10.1016/j.compstruc.2009.07.004

Pedersen P (2006a) A direct analysis of elastic contact using super elements. Computational mechanics 37(3):221–231, DOI 10.1007/s00466-005-0707-0

Pedersen P (2006b) On shrink fit analysis and design. Computational Mechanics 37(2):121–130

Poutiainen I, Tanskanen P, Marquis G (2004) Finite element methods for structural hot spot stress determination - a comparison of procedures. International journal of fatigue 26(11):1147–1157

Reusner H (1987) The logarithmic roller profile - the key to superior performance of cylindrical and taper roller bearings. Ball bearing journal 230:2–10

Truman CE, Booker JD (2007) Analysis of a shrink-fit failure on a gear hub/shaft assembly. Engineering failure analysis 14(4):557–572, DOI 10.1016/j.engfailanal.2006.03.008

White DJ, Humpherson J (1969) Finite-element analysis of stresses in shafts due to interference-fit hubs. Journal of Strain Analysis for Engineering Design 4(2):105–114, DOI 10.1243/03093247V042105